

CRYSTAL CHEMISTRY OF DARK BLUE AQUAMARINE FROM THE TRUE BLUE SHOWING, YUKON TERRITORY, CANADA

LEE A. GROAT[§]

Department of Earth and Ocean Sciences, University of British Columbia, Vancouver, British Columbia V6T 1Z4, Canada

GEORGE R. ROSSMAN

Division of Geological and Planetary Sciences, California Institute of Technology, Pasadena, California 91125-2500, U.S.A.

M. DARBY DYAR

Department of Astronomy, Mount Holyoke College, 50 College Street, South Hadley, Massachusetts 01075, U.S.A.

DAVID TURNER

Department of Earth and Ocean Sciences, University of British Columbia, Vancouver, British Columbia V6T 1Z4, Canada

PAULA M.B. PICCOLI AND ARTHUR J. SCHULTZ

Intense Pulsed Neutron Source, Building 360, Argonne National Laboratory, Argonne, Illinois 60439-4814, U.S.A.

LUISA OTTOLINI

CNR – Istituto di Geoscienze e Georisorse (IGG), Sezione di Pavia, Via Ferrata 1, I-27100 Pavia, Italy

ABSTRACT

Dark blue aquamarine and beryl were discovered at the True Blue showing in the southern Yukon Territory in 2003. Electron-microprobe-derived compositions show up to 5.39 wt.% FeO in the darkest material, which is among the highest Fe concentration known for true beryl. The Al site totals average 2.05, with a maximum of 2.10 *apfu*, which implies that there is more Fe present in the sample than can be accommodated at the Al position. Charge-balance considerations and Mössbauer spectra show that the Fe is present as both Fe²⁺ and Fe³⁺. Optical absorption and Mössbauer spectra and the results of the X-ray and neutron single-crystal refinements suggest that there is very little Fe at the tetrahedral or channel sites. Previous investigators have proposed that the color of blue beryl is due to intervalence charge-transfer (IVCT) between Fe²⁺ and Fe³⁺ cations. The anisotropy of the optical absorption spectra suggest that if the mechanism responsible for the color in our samples is IVCT, the vector between the ions involved must be oriented approximately parallel to *c*. The only vectors that fulfill this condition and have a realistic length (2.300 Å) are 4*d*–Al and 6*g*–Be. Given the close proximity of the Si positions (closer than any anion sites), it is difficult to conceive of the substitution taking place at the interstitial 4*d* site. However, Fe could substitute at the interstitial 6*g* position, but likely only in very small amounts, because of the need to maintain local charge-balance. Unfortunately, there is no evidence of this in the Mössbauer spectra or in difference-Fourier maps of the X-ray- and neutron-diffraction data. For the former technique, it is likely that any doublet arising from Fe in the 6*g*O₆ polyhedron is too similar to the Fe in the AlO₆ octahedra to be resolved for either Fe²⁺ or Fe³⁺. Calculations suggest that the concentration of Fe involved in the IVCT process is 0.08 *apfu* Fe, of which half (0.04 *apfu*, 0.17 *e*⁻) would potentially be at the interstitial site. This amount of electrons and this nuclear density are likely too small to be seen on the difference-Fourier maps.

Keywords: aquamarine, beryl, color, electron microprobe, optical absorption, Mössbauer spectroscopy, X-ray diffraction, neutron diffraction, Yukon Territory, Canada.

[§] E-mail address: lgroat@eos.ubc.ca

SOMMAIRE

Du béryl bleu foncé (aiguemarine) a été découvert à l'indice True Blue dans le sud du territoire du Yukon en 2003. Les données obtenues avec une microsonde électronique montrent que la teneur en fer atteint 5.39% FeO (poids) dans les cristaux les plus foncés, ce qui serait la plus forte concentration connue pour le béryl. Le site *Al* contient en moyenne 2.05, et un maximum de 2.10 *apfu*, ce qui implique qu'il y a plus de Fe dans l'échantillon que ne pourrait être accommodé au site *Al*. D'après le bilan des charges et les spectres Mössbauer, le fer serait présent sous forme de Fe^{2+} et de Fe^{3+} . Les spectres d'absorption optique et de Mössbauer et les résultats d'affinements de la structure par diffraction des rayons X et des neutrons démontrent qu'il y a que très peu de fer au site tétraédrique ou dans les canaux. Les chercheurs antérieurs avaient proposé que la couleur du béryl bleu serait due à un transfert de charges intervalences entre les cations Fe^{2+} et Fe^{3+} . D'après l'anisotropie des spectres d'absorption optique, ce mécanisme pourrait être responsable de la couleur dans nos échantillons si le vecteur entre les ions impliqués sont orientés à peu près parallèles à *c*. Les seuls vecteurs qui puissent satisfaire cette condition tout en ayant des longueurs réalistes (2.300 Å) sont *4d-Al* et *6g-Be*. Compte tenu de la proximité des positions *Si* (inférieures à n'importe quel site anionique), il est difficile de concevoir une substitution au site interstitiel *4d*. Toutefois, le fer pourrait substituer au site interstitiel *6g*, mais probablement en quantités très restreintes, à cause de la nécessité d'imposer l'électroneutralité à l'échelle locale. Malheureusement, il n'y a aucune évidence d'une telle substitution dans les spectres Mössbauer ou dans les projections de différence-Fourier des données acquises par diffraction X et diffraction neutronique. Selon la technique Mössbauer, il semble probable que tout doublet attribuable au Fe dans le polyèdre 6gO_6 est trop semblable au fer dans les octaèdres *AlO*₆ pour que puissent être résolus soit le Fe^{2+} ou le Fe^{3+} . Nos calculs montrent que la concentration de Fe impliquée dans le transfert de charges intervalences est 0.08 *apfu* Fe, et de cette quantité, seule la moitié (0.04 *apfu*, 0.17 *e*⁻) pourrait loger au site interstitiel. Cette quantité d'électrons et cette densité nucléaire seraient probablement trop faibles pour être évidentes dans les projections de différence-Fourier.

(Traduit par la Rédaction)

Mots-clés: aiguemarine, béryl, couleur, microsonde électronique, absorption optique, spectroscopie Mössbauer, diffraction X, diffraction neutronique, Territoire du Yukon, Canada.

INTRODUCTION

Dark blue beryl and aquamarine were discovered at the True Blue showing in the southern Yukon Territory in 2003 (Rohtert *et al.* 2003). The geology and origin of the occurrence are described by Turner (2006) and Turner *et al.* (2007). The crystals occur in a swarm of closely spaced quartz ± siderite ± fluorite ± allanite veins that fill tension gashes in a Mississippian-age (~360 Ma) syenite stock. The veins range in thickness from 0.5 to 20 cm, and locally comprise up to 30% of the rock. The vein zone measures 700 × 400 m in outcrop at the surface, and is exposed over an elevation range of 100 m. Within this area, more than 200 individual occurrences have been discovered.

The beryl crystals range in size from a few mm to 5 × 2.5 cm, and in color from pale to medium green and from pale to dark blue. Some of the crystals, especially those occurring with allanite, show a blue core and a green rim. Because dark blue beryl is rare in nature, efforts in the field concentrated on this material. According to Rohtert *et al.* (2003), the dark blue color is maintained at exceptionally small sizes for aquamarine. Material gathered from the surface showed abundant fractures that limit the size of faceted stones. Microscopic examination revealed that most samples are also fairly heavily included, which significantly affects their transparency (Rohtert *et al.* 2003). Internal features include fractures, "fingerprints," growth tubes, two-phase fluid + gas inclusions, and transparent, nearly colorless quartz crystals. One of the small stones has a

surface-reaching inclusion of siderite surrounded by a thin layer of pyrrhotite (Rohtert *et al.* 2003).

Although rare, dark blue aquamarine crystals have been recovered from a pegmatite in migmatite at the Tatu mine, Minas Gerais, Brazil (Lageoiro *et al.* 2004), and from the Ambositra beryl-columbite pegmatite (Pezzotta 2001) in Madagascar. Proctor (1984) described the discovery (in 1964) of dark blue aquamarine fragments totaling 22 kg in the Marambaia Valley in Brazil. Proctor (1984) also described a 34.7 kg crystal (dubbed the "Marta Rocha" crystal) that ultimately yielded 57,200 carats of dark blue aquamarine, and Viana *et al.* (2002b) reported dark blue beryl from pegmatites near Pedra Azul, Minas Gerais, Brazil. In most of these reports, neither quantitative spectra nor color measurements are presented, so it is difficult to judge the relative darkness of these samples.

There are, however, several reports of high Fe-content beryl with quantitative analyses. Turner *et al.* (2007) reported up to 5.92 wt.% FeO in dark blue beryl from the True Blue locality. Beryl crystals with high iron contents have also been reported from the Calcaferro mine in Italy (3.83 wt.% FeO, Aurisicchio *et al.* 1988; 6.22 wt.% Fe₂O₃, Duchi *et al.* 1993); Monte Cervandone in Italy (4.62 wt.% FeO, Aurisicchio *et al.* 1988), the Lassur mine, Ariège, France, (3.23 wt.% Fe₂O₃ and 0.22 wt.% FeO, Fontan & Fransolet 1964), the Bountiful Beryl pegmatite, Mohave County, Arizona (2.24 wt.% FeO and 2.08 wt.% Fe₂O₃, Schaller *et al.* 1962) and from conglomerates in southeastern Ireland (2.03 wt.% FeO and 2.00 wt.% Fe₂O₃, Sanders & Doff

1991). All of these beryl samples were reported to be blue in color.

Other members of the beryl family with high iron contents are stoppanite, which occurs in mirolitic cavities in volcanic ejecta at Latium, Italy, and contains up to 19.30 wt.% Fe₂O₃ (Della Ventura *et al.* 2000), and bazzite from Val Strem with 8.3 wt.% Fe₂O₃ (Nowacki & Phan 1964). Both are light blue in color.

We undertook this study to characterize the role of iron in the crystal structure of this beryl and to speculate on the origin of the dark blue color.

PREVIOUS WORK

Most previous investigators of the role of iron in the crystal structure of beryl have used Mössbauer spectroscopy. Price *et al.* (1976) reported that 4.2 K Mössbauer spectra of beryl contain three doublets with isomer shifts of 1.3, 1.0, and ~0.6 mm/s and quadrupole splittings of 2.7, 1.5, and ~0.7 mm/s, respectively. They interpreted the first (outermost) Fe²⁺ doublet to represent octahedral Fe²⁺ at the *Al* site. The middle doublet was assigned on the basis of its isomer shift to be tetrahedral Fe²⁺, but it was unclear if the site involved was the distorted *Be* site (slightly preferred) or the *Si* site. Their (innermost) Fe³⁺ doublet was poorly resolved. The 810 nm optical band was found to be associated with the tetrahedral doublet.

Parkin *et al.* (1977) reported a single 295 K Mössbauer spectrum of beryl showing the presence of both Fe²⁺ and Fe³⁺, but their data were not of sufficient quality (owing to a low concentration of Fe in their sample) for Mössbauer parameters to be determined. Goldman *et al.* (1978) suggested that the inner Fe²⁺ doublet arises from Fe²⁺ at the channel site (rather than a tetrahedral site), by analogy with the inner doublet in the cordierite spectrum. Their site assignments were supported by the work of Goncharov *et al.* (1985).

Braga *et al.* (2002) used Mössbauer spectroscopy to study emerald from two localities in Brazil. They concluded that Fe²⁺ and Fe³⁺ substitute at both the octahedrally coordinated *Al* site and the tetrahedrally coordinated *Be* site.

Viana *et al.* (2002a) obtained Mössbauer spectra from several specimens of blue beryl in the temperature range of 4.2 to 500 K. All of the room-temperature spectra showed an asymmetric Fe²⁺ doublet ($\Delta E_Q \sim 2.7$ mm/s, $\delta \sim 1.1$ mm/s), with a very broad low-velocity peak. The asymmetry was attributed to a relaxation process involving Fe²⁺ and H₂O molecules in the structural channels, as suggested by Price *et al.* (1976). The spectrum at 500 K also showed a broad but symmetrical doublet, with a clear splitting of the lines indicating the presence of at least two Fe²⁺ components. At 4.2 K, the spectrum of a sample of deep blue beryl was fit with four symmetrical doublets, one of which could be related to Fe²⁺ in the structural channels. Ferrous iron was found to occupy both octahedral and tetrahe-

dral sites, whereas Fe³⁺ was considered to occupy the octahedral position. Viana *et al.* (2002a) concluded that color in beryl is dictated by the relative proportions of Fe³⁺ at the octahedral sites and of Fe²⁺ in the channels. Deep blue samples were reported to contain little Fe³⁺. These conclusions were echoed by Viana *et al.* (2002b), in which aquamarine samples from pegmatites of Minas Gerais, Brazil, were characterized by chemical analysis, infrared and UV-visible spectroscopy, thermal analysis, and high-temperature X-ray diffraction.

Lagoeiro *et al.* (2004) reported Mössbauer results for dark blue beryl (with FeO up to 1.68 wt.%) from the Tatu mine in Brazil. The results are similar to those of Price *et al.* (1976) and suggest 70% Fe²⁺ and 30% Fe³⁺, with both Fe²⁺ and Fe³⁺ at the *Al* site, and additional Fe²⁺ in tetrahedral coordination.

Da Costa *et al.* (2006) obtained Mössbauer spectra from a sample of blue beryl containing ~9,000 ppm Fe at 295 and 500 K. The room-temperature spectrum showed the presence of an asymmetric Fe²⁺ doublet ($\Delta E_Q \sim 2.7$ mm/s, $\delta \sim 1.1$ mm/s) with a very broad low-velocity peak. These features were interpreted to result from Fe²⁺ at three different crystallographic sites (octahedral, tetrahedral, and channel). There was no clear evidence for Fe³⁺. Thermal treatment at 500 K caused no significant changes in the Mössbauer spectra. The authors reported that above ~1100 K, most of the Fe²⁺ ions are oxidized.

Khaibullin *et al.* (2003) implanted colorless beryl crystals with 40 keV Fe⁺ ions and then annealed them at 600°C for 30 m. Optical absorption, Mössbauer, and Rutherford back-scattering spectroscopies showed Fe²⁺ replacing Be at the tetrahedrally coordinated *Be* positions and Fe³⁺ substituting for Al at the octahedrally coordinated *Al* sites.

Figueiredo *et al.* (2008) used X-ray absorption spectroscopy at the Fe *K*-edge to study blue beryl crystals from the Licungo pegmatite in Mozambique. The results suggest that Fe replaces Al at the octahedrally coordinated *Al* sites, and the authors proposed that this substitution is possibly responsible for the blue color.

Adamo *et al.* (2008) used various techniques including infrared spectroscopy and single-crystal X-ray diffraction to study synthetic dark blue beryl containing 1.95 wt.% Fe₂O₃ and 1.98 wt.% CuO. They reported that Cu substitutes for Be at the *Be* site and Fe for Al at the *Al* position.

There have been a handful of studies of the causes of blue color in beryl, and several reports of its optical absorption spectra. Loeffler & Burns (1978), Platonov *et al.* (1978) and Goldman *et al.* (1978) recognized that the deep blue color is due to intervalence charge-transfer (IVCT) between Fe²⁺ cations at the *Al* sites and small amounts of Fe³⁺ in another site that produces an absorption band centered near 620 nm in the E ∥ c direction. Normally, interpretation of Fe²⁺-Fe³⁺ IVCT is easily accomplished in terms of identification of the sites of the participating cations. However, in the case of beryl,

there is no normally occupied site at an appropriate distance near the *Al* site in the appropriate direction (parallel to the *c* axis). Consequently, Platonov *et al.* (1978, 1979a, 1979b, 1979c) specifically suggested that the small amounts of Fe^{3+} are at the 6*g* position ($1/3, 2/3, 1/2$), a location with six-fold (trigonal prismatic) coordination that lies between the *Al* sites and is normally empty (Figs. 1a, b). Platonov *et al.* (1978, 1979a, 1979b, 1979c) also suggested that cations at the 4*d* site ($0, 1/2$) might influence the color of beryl; this site has fourfold (square planar) coordination, lies between the *Be* sites, and is normally empty as well (Figs. 1a, b).

All subsequent investigators (*e.g.*, Taran *et al.* 1989) have accepted the IVCT origin of the 620 nm band. However, no crystallographic studies were conducted on samples with enough iron to confirm or deny the occupation of Fe^{3+} in the normally empty sites.

The question of the Fe^{2+} occupancy and the interpretation of the optical and Mössbauer spectra have also been somewhat problematic. A pair of bands in the optical spectrum near 820 and 970 nm that is more intense in the $\text{E} \parallel c$ direction is particularly typical of Fe^{2+} in an octahedral site (Goldman *et al.* 1978, Price *et al.* 1976). Whereas the interpretation of these bands is not controversial, they are often buried under a much more intense band near 820 nm. The iron responsible for the intense 820 nm band is correlated with a weaker band near 2100 nm, and is also correlated with the inner doublet in the Mössbauer spectrum (Price *et al.* 1976). The large separation between the two components indicated that the site is significantly distorted from either ideal octahedral or tetrahedral symmetry (Goldman *et al.* 1978). Price *et al.* (1976) suggested that it represents Fe^{2+} in the tetrahedral site, and Goldman *et al.* (1978)

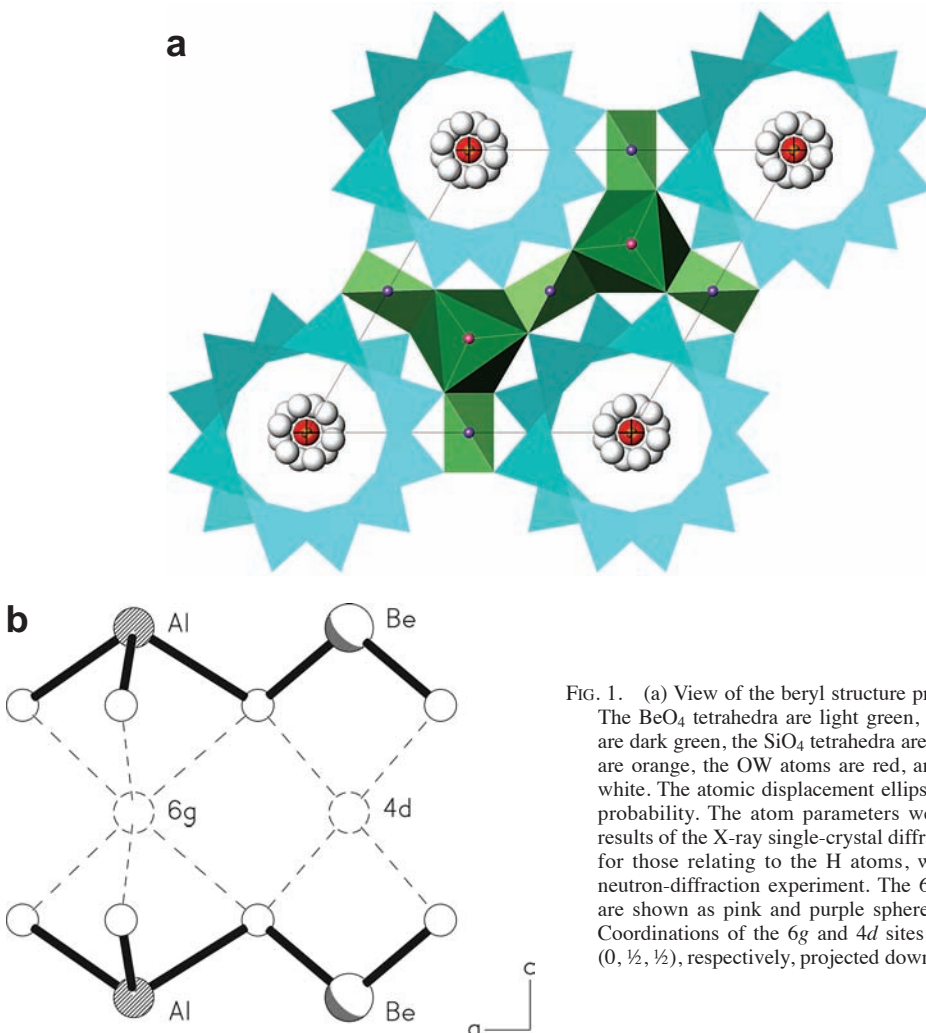


FIG. 1. (a) View of the beryl structure projected onto (001). The BeO_4 tetrahedra are light green, the AlO_6 octahedra are dark green, the SiO_4 tetrahedra are blue, the Na atoms are orange, the OW atoms are red, and the H atoms are white. The atomic displacement ellipsoids represent 50% probability. The atom parameters were taken from the results of the X-ray single-crystal diffraction study, except for those relating to the H atoms, which are from the neutron-diffraction experiment. The 6*g* and 4*d* positions are shown as pink and purple spheres, respectively. (b) Coordinations of the 6*g* and 4*d* sites at ($1/3, 2/3, 1/2$) and ($0, 1/2, 1/2$), respectively, projected down [010] (*c* vertical).

suggested that it could represent Fe^{2+} in a channel site in the silicate ring. Subsequent investigators have invoked both interpretations. Taran & Rossman (2001) presented a systematic investigation of the optical spectra of Fe^{2+} in tetrahedral sites of various distortions and concluded

that the 820 and 2100 nm bands of the beryl spectrum are fully compatible with what would be expected if Fe^{2+} occupied the distorted tetrahedral Be site of the beryl structure.

None of these investigators have definitively settled the details of the origin of the strongly $E \parallel c$ polarized band at 620 nm, nor have they conclusively demonstrated where the non-octahedral Fe^{2+} resides. It was in the hope of addressing these issues with the high Fe-content True Blue showing beryl that this investigation was initiated.

TABLE 1. AVERAGE COMPOSITIONS OF SELECTED SAMPLES OF BERYL FROM THE TRUE BLUE SHOWING

Sample	46 EMPA mount	38 EMPA mount	56 EMPA mount	GS2 EMPA mount	GS2 Neutron crystal	GS2 X-ray crystal
Color	Medium blue	Medium blue	Medium blue	Dark blue	Dark blue	Dark blue
<i>n</i>	13	11	10	10	25	8
SiO_2 wt. %	63.13	62.59	62.79	62.36	62.56	62.51
TiO_2	0.00	0.01	0.00	0.02	0.02	0.03
Al_2O_3	13.25	13.15	13.66	12.80	12.25	11.98
Sc_2O_3	0.01	0.01	0.05	0.02	0.02	0.00
BeO^*	13.13	13.02	13.08	13.00	12.98	12.98
MgO	2.61	2.09	1.65	1.89	1.85	1.91
FeO	2.36	3.12	3.26	4.67	4.89	5.39
Na_2O	2.20	2.27	2.20	1.99	2.31	2.32
$\text{H}_2\text{O}^\dagger$	3.35	3.42	3.35	3.17	2.80	2.81
Total	100.04	99.76	100.08	99.96	99.73	99.93
Si <i>apfu</i>	6.003	6.001	5.994	5.993	6.017	6.017
Ti	0.001	0.001	0.000	0.001	0.001	0.002
Al	1.484	1.485	1.536	1.449	1.389	1.359
Sc	0.002	0.001	0.004	0.001	0.002	0.000
Be	3.000	3.000	3.000	3.000	3.000	3.000
Mg	0.370	0.299	0.235	0.271	0.265	0.274
Fe_{tot}	0.188	0.251	0.261	0.376	0.394	0.434
Na	0.405	0.423	0.407	0.371	0.431	0.433
Al site	2.043	2.036	2.032	2.098	2.049	2.069
Mg + Fe <i>tot</i>	0.558	0.550	0.495	0.648	0.659	0.707
$\text{Fe}^{2+}_{\text{calc}}^\ddagger$	0.153	0.120	0.172	0.099	0.166	0.159
$\text{Fe}^{3+}_{\text{calc}}^\ddagger$	0.035	0.131	0.089	0.277	0.228	0.274
SIMS data [§]						
BeO (wt. %)	14.40			14.18		
Li_2O	0.009			0.012		
H_2O	1.61			1.85		
LAM-ICP-MS data						
Li (ppm)						17.8
B						58.10
K						24.6
Ca						1130
Sc						45.3
Ti						153.1
V						9.84
Cr						2.54
Mn						6.97
Cs						15.01

Note: For the electron-microprobe analyses the following standards were used: albite (SiKa, AlKa, NaKa), rutile (TiKa), Sc metal (ScKa), diopside (MgKa), and fayalite (FeKa). Vanadium, Cr, Ca, Mn, K, and Cs were sought, but not detected. Compositions were recalculated on the basis of 3 Be and 18 O *apfu*.

* Determined by stoichiometry.

† Calculated using $\text{H}_2\text{O} = (0.84958 \times \text{Na}_2\text{O}) + 0.8373$ (G. Giuliani, pers. commun.).

‡ $\text{Fe}^{2+}_{\text{calc}} = \text{Fe}_{\text{tot}} - (\text{Na} - \text{Mg})$; $\text{Fe}^{3+} = \text{Fe}_{\text{tot}} - \text{Fe}^{2+}_{\text{calc}}$.

§ *n* = 10 for sample 46 and 9 for sample GS2; calibration standards were danalite (Be) and beryl samples from Aurisicchio *et al.* (1988) (H_2O).

|| *n* = 3 for all elements except B, for which *n* = 2.

SAMPLES

The following blue beryl samples from the showing were selected for study: 38, 46, 56, and GS2 ("grade sample 2"). In sample 38, medium-blue beryl crystals up to 15×3 mm occur with siderite in quartz veins in intermediate syenite. Sample 46 consists of transparent medium-blue beryl crystals up to 7×4 mm occurring with calcite in quartz veins cutting mafic syenite. The beryl crystals in sample 56 are medium blue in color, up to 5×2 mm in size, and occur with clear fluorite and chlorite in quartz veins in mafic syenite. The GS2 sample consists of dark turquoise to dark blue beryl crystals up to 38×11 mm in size that occur with abundant manganiferous siderite and minor clear to dark purple fluorite in quartz veins 2–7 mm wide in tan syenite. A total of 57.9 g of beryl was collected from a 65 kg bulk sample from this occurrence. Details of the experimental methods are given in the Appendix.

RESULTS

Compositions

Turner *et al.* (2006) showed that beryl from the True Blue showing contains high concentrations of Fe (to 0.48 *apfu*, corresponding to 5.92 wt.% FeO if all of the Fe is assumed to be ferrous), Mg (also to 0.48 *apfu*, 3.42 wt.% MgO), Na (to 0.49 *apfu*, 2.66 wt.% Na_2O), and calculated H_2O (to 3.10 wt.%). The FeO concentration is among the highest known for true beryl.

Average electron-microprobe-derived compositions of the samples used in this study are given in Table 1. The compositions show that the dark blue GS2 samples contain significantly more Fe (to 0.43 *apfu*, corresponding to 5.39 wt.% FeO if all of the Fe is assumed to be Fe^{2+}). The Al, Mg, and calculated H_2O concentrations all decrease with increasing Fe, whereas the Si and Na concentrations remain relatively constant. Titanium and Sc contents are close to the detection limit. Table 1 also shows that the average Al site totals, with all Mg and Fe substitution occurring at the Al site, are invariably greater than 2.00 *apfu*, and attain a maximum value of 2.10 *apfu* for GS2 crystals from the EMPA mount.

Numerous previous studies have shown that the charge imbalance created by substitution of a divalent

cation at the *Al* site can be neutralized by substitution of a monovalent cation at a channel site. We assume that all Fe occurs at the *Al* site, and that $\text{Fe}^{2+} + \text{Mg} = \text{Na}$, $\text{Fe}^{2+}_{\text{calc}} = \text{Fe}_{\text{tot}} - (\text{Na} - \text{Mg})$, and $\text{Fe}^{3+}_{\text{calc}} = \text{Fe}_{\text{tot}} - \text{Fe}^{2+}_{\text{calc}}$. As shown in Table 1, $\text{Fe}^{2+}_{\text{calc}} > \text{Fe}^{3+}_{\text{calc}}$ for samples with less Fe but $\text{Fe}^{3+}_{\text{calc}} > \text{Fe}^{2+}_{\text{calc}}$ for the GS2 samples, for which $\text{Fe}^{3+}_{\text{calc}}:\text{Fe}^{2+}_{\text{calc}}$ is approximately 2:1.

Figure 2 shows *Al* versus those elements assumed to substitute for *Al* at the *Al* site, in *apfu*. The data points would normally be expected to scatter about the solid line ($\text{Al} + \text{Mg} + \text{Sc} + \text{Fe}^{2+} + \text{Fe}^{3+} = 2 \text{ apfu}$). However, all of the data points are displaced well above the solid line (on average by 0.05 and as much as $\sim 0.1 \text{ Mg} + \text{Sc} + \text{Fe apfu}$); a linear regression applied to the data results in the equation $(\text{Mg} + \text{Sc} + \text{Fe}) = -1.140(\text{Al}) + 2.256$ ($r^2 = 0.945$). The regression line (dashed in Fig. 2) diverges from the solid line with increasing substitution, which primarily corresponds to increasing Fe concentrations. It is interesting to note that the two lines converge in the opposite direction and ultimately cross at *Al* $\sim 2 \text{ apfu}$. This suggests that there is more Fe present in the sample than can be accommodated at the *Al* position.

Figure 3 shows *Mg* + *Fe* versus *Na*, in *apfu*. The data for most of the samples show a wide range, especially

for *Mg* + *Fe*. The solid line represents $\text{Mg} + \text{Fe} + \text{Na} = 2 \text{ apfu}$, and because the electron-microprobe-compositions show that Na is the only monovalent cation in the structure, the data points would be expected to scatter around this line if all of the Fe was ferrous. The fact that all of the data points lie below the line suggests the presence of considerable Fe^{3+} , and the trend of the points (which is discernable despite the scatter) shows that most of the increase in *Mg* + *Fe* is due to the addition of Fe^{3+} . The positions of the data points representing compositions from the GS2 X-ray crystal (chosen because they show a tight cluster) suggest $\sim 0.425 \text{ Mg} + \text{Fe}^{2+} \text{ apfu}$ and $\sim 0.700 - \sim 0.425 = 0.275 \text{ Fe}^{3+} \text{ apfu}$, similar to the values in Table 1 ($0.433 \text{ Mg} + \text{Fe}^{2+}_{\text{calc}}$ and $0.274 \text{ Fe}^{3+}_{\text{calc}} \text{ apfu}$).

Ion-microprobe-derived compositions were obtained for samples 46 and GS2 (from the EPMA mount) and are listed in Table 1. The BeO concentrations are approximately 1 wt.% higher than those calculated by stoichiometry from the electron-microprobe-derived compositions. This is most likely due to the analytical difficulties associated with relatively high concentrations of Be and lack of suitable standards. The ion-microprobe-derived data also show essentially no Li,

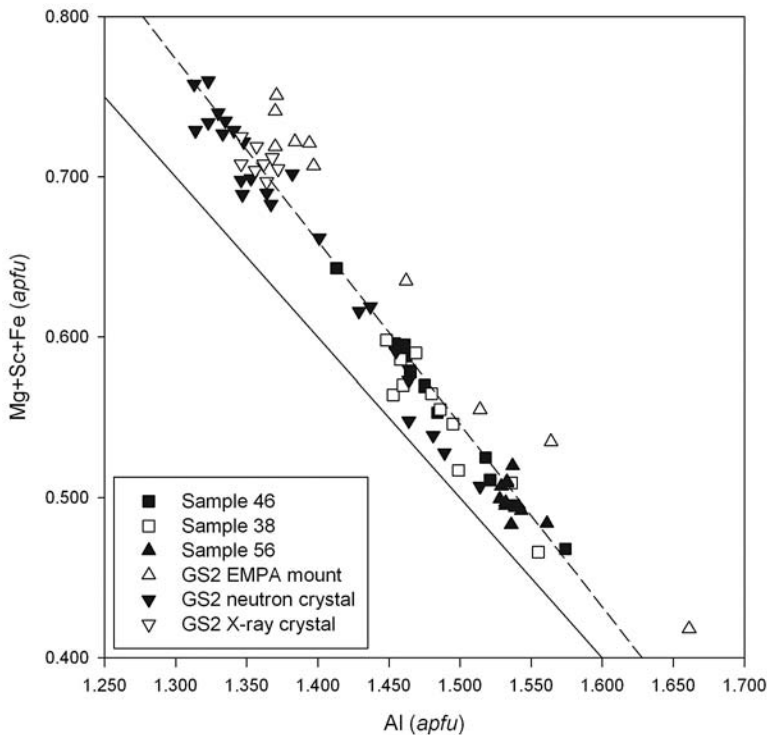


FIG. 2. Concentration of *Al* versus *Mg* + *Sc* + *Fe* (in *apfu*). The solid line represents $\text{Al} + \text{Mg} + \text{Sc} + \text{Fe} = 2 \text{ apfu}$, and the equation for the dashed regression line is $(\text{Mg} + \text{Sc} + \text{Fe}) = -1.140(\text{Al}) + 2.256$ ($r^2 = 0.945$).

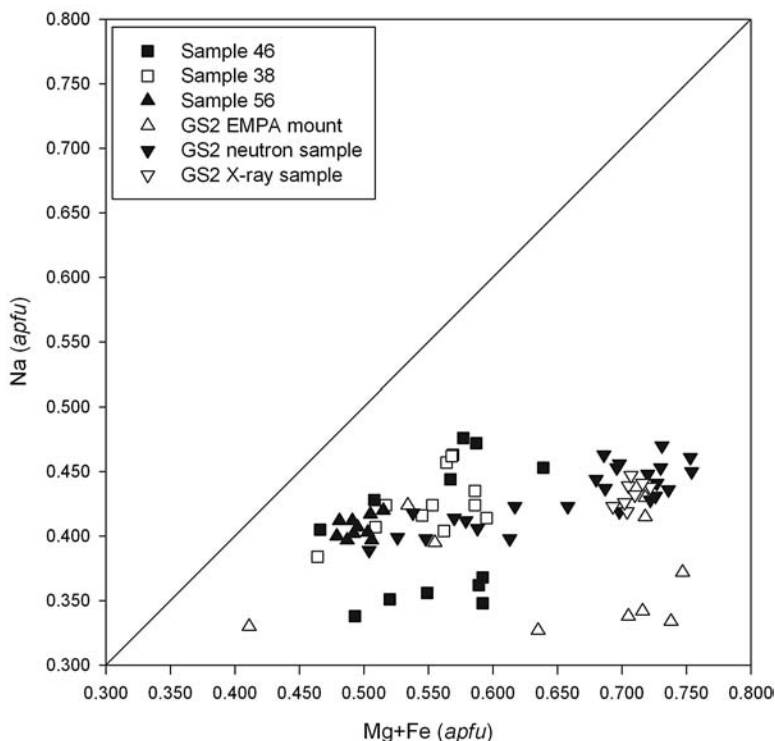


FIG. 3. Concentration of Mg + Fe versus Na (in apfu). The solid line represents Mg + Fe + Na = 1 apfu.

which is important because Li is considered to substitute at the *Be* site in the beryl structure (with charge balance provided *via* monovalent cations at the channel sites).

The LA-ICP-MS compositions (Table 1) confirm the trace Li concentrations seen in the ion-microprobe data and the low concentrations of K, Ca, Sc, Ti, V, Cr, Mn, and Cs seen in the electron-microprobe data. The compositions also show trace concentrations of B, although the results should be considered qualitative owing to the high standard deviation.

Optical absorption spectroscopy

The absorption spectra for sample GS2 (Fig. 4) show high absorption when the electric vector (*E*) is parallel to the *c* axis (*E* ∥ *c*), and comparatively weak absorption in the *E* ⊥ *c* spectrum. The spectrum has the greatest intensity per unit thickness of the *E* ∥ *c* bands of any beryl that we have measured or know about. This accounts for the intense depth of color of crystals from the True Blue locality. Using the ankerite spectrum as a model (<http://minerals.gps.caltech.edu/FILES/Visible/CARBONATE/ankerite6376b.gif>), we conclude that siderite features do not appear to be a

significant contribution to the optical spectrum. The enhancement of the Fe^{2+} bands associated with iron in the octahedral site suggests that the Fe^{3+} is interacting with Fe^{2+} at the *Al* site, and the polarization direction indicates that the Fe^{3+} is situated either directly above or below the *Al* site.

The band (*E* ⊥ *c*) at about 830 nm that Taran & Rossman (2001) assigned to iron at the tetrahedral site is a comparatively weak feature in the spectrum. Because this band has a high molar absorptivity (Goldman *et al.* 1978) yet is weak in the spectrum of beryl from the True Blue showing, the implication is that Fe^{2+} at the tetrahedral site constitutes only a small fraction of the total iron in this sample. Features from Fe^{3+} are intrinsically weak and are essentially swamped by the other features in the spectrum. There is a minor shoulder at about 428 nm in the *E* ∥ *c* spectrum that is appropriately positioned to be attributed to octahedral Fe^{3+} . The band is so weak that it is not possible to use the optical spectrum to obtain an accurate estimate of the small amount of Fe^{3+} in the sample.

The features that dominate the spectrum in Figure 4 have been investigated by previous workers (Taran & Rossman 2001). The absorption in the 500 to 800 nm

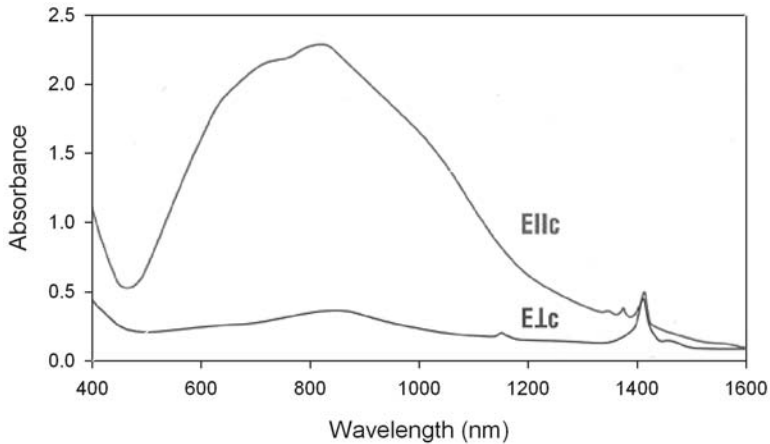


FIG. 4. Visible near-infrared absorption spectra of a slab of sample GS2 0.683 mm thick.

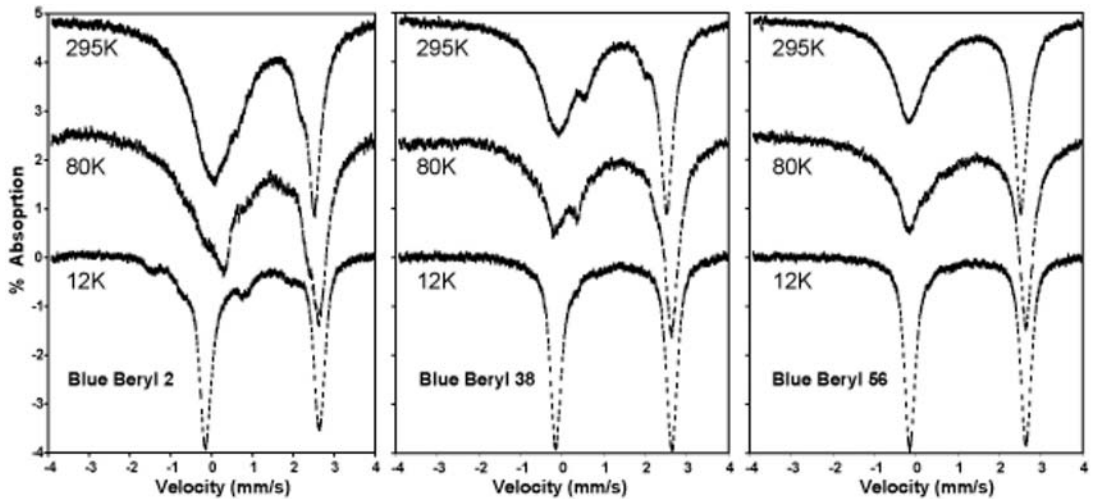


FIG. 5. Mössbauer spectra at 295, 80, and 12 K for samples 38, 56, and GS2.

region originates from an intervalence charge-transfer interaction between Fe^{2+} and Fe^{3+} . On the basis of the bands at about 830 and the Mössbauer fraction of Fe^{2+} (see below), the ϵ value (molar absorption coefficient) of the 1050 nm band is about 12, a value somewhat higher than the value of about 3 calculated for Beryl #1 in Goldman *et al.* (1978). Such enhancement of Fe^{2+} bands has commonly been observed in other minerals where octahedral Fe^{2+} is involved in intervalence charge-transfer with Fe^{3+} (Amthauer & Rossman 1984), but makes it difficult to calculate an exact concentration of Fe^{2+} from the optical spectrum. The enhancement of the Fe^{2+} bands associated with iron in the octahedral site

suggests that the Fe^{3+} is interacting with Fe^{2+} at the Al site, and the polarization direction indicates that the Fe^{3+} is situated either directly above or below the Al site.

Features near 1400 nm arise from channel water in two different orientations with respect to the c axis (Wood & Nassau 1968). The intensity of the spectrum indicates that the concentration of water in the beryl is comparable to, or somewhat higher than, what is commonly observed in blue beryl. Intensities of the Type-1 bands ($E \parallel c$) are lower than the Type-2 bands ($E \perp c$) indicating the greater proportion of water bound to Na in the channel. The infrared spectra in the 6000 to 2200 cm^{-1} region (not shown) confirm that the

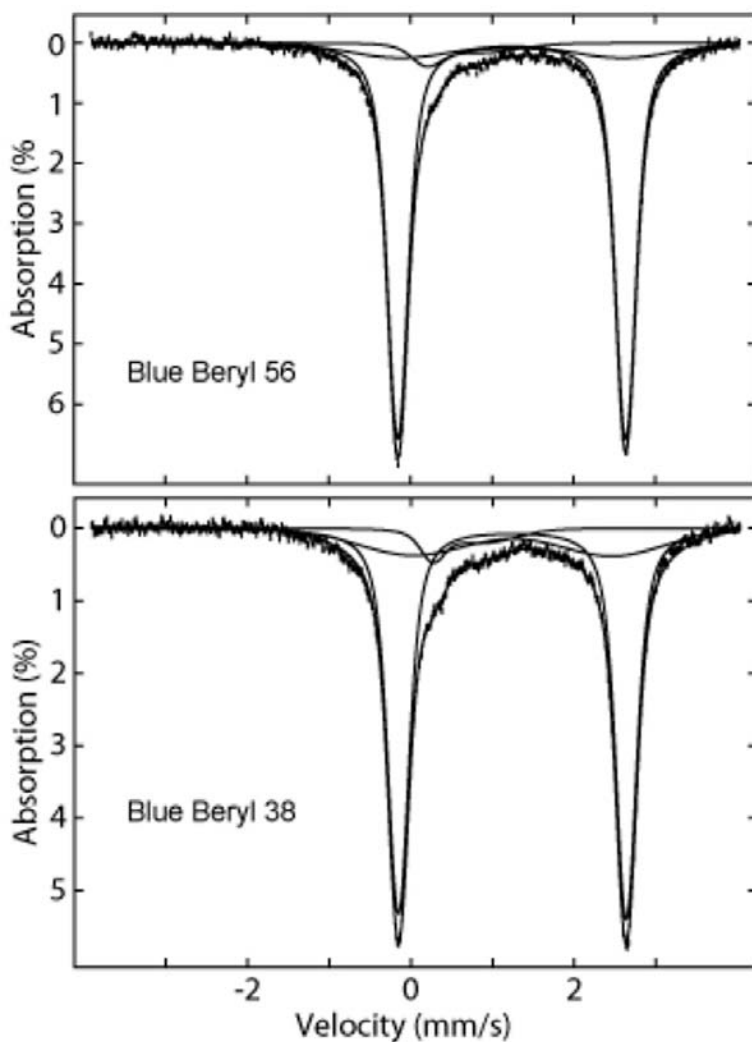


FIG. 6. Quadrupole splitting distribution (QSD) fits to 4 K Mössbauer spectra for samples 38 and 56.

beryl has relatively high water content dominated by type-II water.

Mössbauer spectroscopy

The previously published Mössbauer spectra contrast with the spectra of the three samples studied here, shown in Figures 5 and 6. It is immediately apparent that our 4 K and 12 K spectra do not contain an inner Fe^{2+} doublet with parameters of $\delta = 1.13$ mm/s and $\Delta = 1.46$ mm/s (cf. Fig. 2 in Price *et al.* 1976 and Fig. 1 in Goncharov *et al.* 1985). This would have been

the doublet assigned by those investigators to Fe^{2+} either in tetrahedral coordination or in the channels.

Given the pronounced asymmetry of the Mössbauer doublets above 20 K, as observed by all previous investigators, we fit only the 4 K and 12 K spectra; note that the fits to the data for sample GS2 were greatly complicated by the presence of microcrystalline siderite. The parameters of the resultant fits to 4 K and 12 K data are given in Table 2; fits for 4 K data from samples 38 and 56 are shown in Figure 6. We observed only a single paramagnetic doublet for Fe^{2+} , with parameters closely corresponding to those described by Price *et al.* (1976) for octahedral Fe^{2+} at the Al site: $\delta = 1.24$ – 1.30

mm/s and $\Delta = 2.75\text{--}2.79$ mm/s. We found no evidence for a second Fe^{2+} doublet in any of the three samples studied. Approximately 4–16% of the total Fe is present as Fe^{3+} , and it appears that sample GS2 has the highest percentage of Fe^{3+} relative to the total Fe content, although much less than is suggested by the electron-microprobe-derived compositions. Our Fe^{3+} doublet has parameters that are appropriate only for octahedral Fe^{3+} , and thus we tentatively assign Fe^{3+} to the *Al* site as well.

Unfortunately, like previous workers, we have no explanation for the pronounced asymmetry of the Mössbauer spectra at temperatures above 4 K. Were it not for the fact that the X-ray- and neutron-diffraction refinements of the structure (see below) show Fe only at the *Al* site, we might suggest that the high isomer shift of the Fe^{2+} doublet (1.30 mm/s at 12 K) could be due to a coordination polyhedron larger than the AlO_6 octahedron, such as might be found in the channel. The channels might then have some characteristic that would cause the asymmetry.

Unit-cell dimensions

The unit-cell dimensions refined from powder X-ray-diffraction data for the GS2 sample are: a 9.2782(3), c 9.1882(4) Å, V 685.00(6) Å³, $c/a = 0.990$. These compare well with the cell dimensions from the X-ray and neutron single-crystal diffraction studies (Table 3).

TABLE 2. MÖSSBAUER PARAMETERS FOR 4 AND 12 K SPECTRA OF DARK BLUE BERYL

T (K)	ID	#2		#38		#56	
		4	12	4*	12*	4 [†]	12 [†]
Γ	siderite	0.75	0.75				
Δ	sextet	-0.28	-0.23				
δ		0.57	0.44				
B_{eff}		510	493				
A (%)		15	15				
Γ	siderite	0.80	0.70				
Δ		2.10	2.11				
δ		1.29	1.26				
B_{eff}		186	187				
A (%)		21	19				
Γ	Fe^{2+}	0.30	0.33	0.27	0.32	0.27	0.30
Δ		2.77	2.76	2.75	2.79	2.75	2.79
δ		1.30	1.27	1.28	1.24	1.28	1.24
A (%)		49	50	88	88	94	92
Γ	Fe^{3+}	0.67	0.70	0.50	0.50	0.35	0.74
Δ		0.79	0.68	0.79	0.75	0.86	0.80
δ		0.51	0.51	0.49	0.45	0.43	0.41
A (%)		16	16	8	6	4	7
χ^2	—	3.97	8.11	2.20	2.60	2.43	2.28

* These spectra have a 4–6% contribution from unresolved Fe^{2+} that is partially magnetically split. † These spectra have a 1–2% contribution from unresolved Fe^{2+} that is partially magnetically split. Sextets represent contributions from siderite impurities.

The unit-cell dimensions of beryl are correlated with chemical composition, and consequently beryl crystals may be classified according to their c/a ratio. As shown in Figure 7, the a parameter (and volume) for the GS2 sample is higher, and the c/a ratio (0.989) is lower, than most of the values in the literature. In particular, the c/a ratio is lower than the stated range of 0.991–0.996 for “octahedral” beryl where $\text{Al} \leftrightarrow \text{Me}$ represents the main scheme of substitution (Aurischio *et al.* 1988). The only samples with lower c/a values are the hydrous and sodic blue beryl from Ireland described by Sanders & Doff (1991) and the blue beryl from the Calcaferro mine described by Duchi *et al.* (1993).

Crystal-structure refinement from X-ray data

Miscellaneous data about the collection and refinement for both X-ray and neutron experiments are given in Table 3, positional coordinates and anisotropic and equivalent isotropic displacement factors, in Table 4, and interatomic distances and angles, in Table 5. Tables listing the observed and calculated structure-factors may be obtained from the Depository of Unpublished Data on the MAC website [document True Blue CM48_597].

The occupancies of the *B*, *Si*, O(1), and O(2) sites were refined, and the results in each case indicate that they are fully occupied by their namesake species. Subsequently, the occupancies of these positions were fixed.

Aluminum (representing *Al* + *Mg*, which have approximately the same scattering curve for X rays) and Fe were refined at the *Al* site; the results show 1.667(8) *Al* (+ *Mg*) and 0.323(8) *Fe apfu*. The value for

TABLE 3. INFORMATION ON DATA COLLECTION AND STRUCTURE REFINEMENT OF DARK BLUE BERYL

	X-ray	Neutron
a (Å)	9.2909(3)	9.258(3)
c (Å)	9.1996(3)	9.156(3)
V (Å ³)	687.73(4)	679.63(4)
Space group	$P6/mcc$	$P6/mcc$
Z	6	6
Crystal size (mm)	$0.25 \times 0.25 \times 0.25$	$2.00 \times 2.00 \times 3.00$
Radiation	$\text{MoK}\alpha$	Neutrons
Monochromator	graphite	
Temperature (K)	293	20
Total F_o	24547	3605
Unique F_o	364	892
$F_o > 4\sigma F_o$	360	815
R_{int}	0.022(5)	0.08(6)
L.s. parameters	39	38
R_1 for $F_o > 4\sigma F_o$	0.0162	0.0559
R_1 , all unique F_o	0.0164	0.0669
wR_2	0.0459	0.1113
a	0.0221	0.0333
b	0.34	3.19
GoodF (= S)	1.294	1.161

Note: $w = 1/[\sigma^2(F_o^2) + (a \times P)^2 + b \times P]$, where $P = [\text{Max}(F_o^2, 0) + 2 \times F_o^2] / 3$.

TABLE 4. ATOM PARAMETERS FOR DARK BLUE BERYL

		x	y	z	sof	U_{11}	U_{22}	U_{33}	U_{12}	U_{13}	U_{23}	U_{eq}
Be	X	1/2	0	1/4	0.25	0.0096(7)	0.008(10)	0.0078(8)	0.0041(5)	0	0	0.0087(4)
	N	1/2	0	1/4	0.25	0.0078(2)	0.0074(2)	0.0067(3)	0.0037(1)	0	0	0.0073(1)
Al	X	1/3	2/3	1/4	Al 0.1397(7) Fe 0.0270(7)	0.0055(2)	0.0055(2)	0.0065(3)	0.0027(1)	0	0	0.0058(2)
	N	1/3	2/3	1/4	Al* 0.138(2) Fe 0.029(2)	0.0056(4)	0.0056(4)	0.0056(6)	0.0028(2)	0	0	0.0056(4)
Si	X	0.38506(4)	0.11197(4)	0	0.5	0.0060(2)	0.0055(2)	0.0059(2)	0.0031(1)			0.0057(1)
	N	0.3855(1)	0.1123(1)	0	0.5	0.0057(3)	0.0052(3)	0.0050(3)	0.0029(2)	0	0	0.0052(2)
O(1)	X	0.3044(1)	0.2300(1)	0	0.5	0.0144(5)	0.0121(5)	0.0194(5)	0.0100(4)	0	0	0.0138(2)
	N	0.3047(1)	0.2302(1)	0	0.5	0.0118(3)	0.0112(3)	0.0151(4)	0.0089(2)	0	0	0.0113(2)
O(2)	X	0.49435(9)	0.14133(9)	0.14509(8)	1.0	0.0134(4)	0.0130(3)	0.0079(3)	0.0084(3)	-0.0024(2)	-0.0003(3)	0.0106(2)
	N	0.49500(8)	0.14196(8)	0.14519(7)	1.0	0.0110(2)	0.0124(2)	0.0061(2)	0.0080(2)	-0.0011(2)	-0.0006(2)	0.0089(1)
Na	X	0	0	0	0.0354(7)	0.011(1)	0.011(1)	0.028(2)	0.0055(7)	0	0	0.017(1)
	N	0	0	0	0.036(3)	0.009(2)	0.009(2)	0.015(4)	0.004(1)	0	0	0.011(2)
OW	X	0	0	1/4	0.076(4)	0.060(4)	0.060(4)	0.028(3)	0.030(2)	0	0	0.049(3)
	N	0	0	1/4	0.076(2)	0.021(1)	0.021(1)	0.014(1)	0.0105(5)	0	0	0.0186(8)
H	X	0.0(1)	0.09(2)	0.19(1)	0.15(3)	0.05						
	N	0.025(4)	0.094(3)	0.181(3)	0.152(4)	0.052(5)						

sof: site-occupancy factor. X: X-ray, N: Neutron; Al* = (Mg + Al) with a constant Mg:Al ratio of 0.160:0.840.

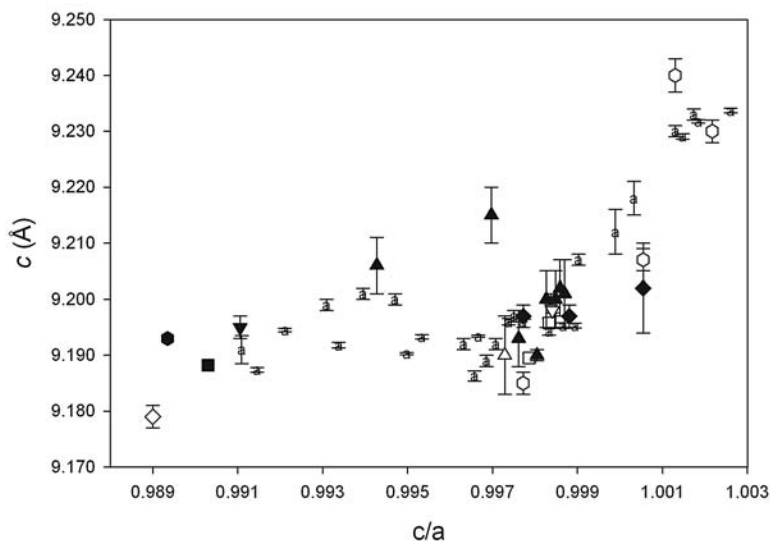


Fig. 7. Values of c/a versus c from the powder diffraction data for sample GS2, compared with powder and single-crystal X-ray and neutron data from the recent literature. Symbols: ■ GS2, this study, □ Pankrath & Langer (2002), ▲ Viana *et al.* (2002b), △ Charoy *et al.* (1996), ▼ Artioli *et al.* (1995), ▽, Schmetzer & Bernhardt (1994), ◆ Artioli *et al.* (1993), ◇ Duchi *et al.* (1993), ● Sanders & Doff (1991), ○ Sherriff *et al.* (1991), a Aurisicchio *et al.* (1988).

Al (+ Mg) is similar to that obtained by electron-probe micro-analysis (1.633 *apfu*; Table 1), but the value for Fe is approximately 0.1 *apfu* lower than that obtained by EPMA (0.434 *apfu*).

Sodium was refined at the 2*b* (0,0,0) position, as is normally the case for alkali-bearing beryl (Sherriff *et al.* 1991). The results show 0.425(9) Na *apfu*, which is similar to that from the electron-microprobe compositions (0.433 Na *apfu*). Oxygen from water molecules was refined at the 2*a* (0,0,½) site to 0.91(4) *apfu*. Hydrogen was refined at the position determined by refinement of the neutron-diffraction data (see below), with the isotropic displacement parameter constrained to 0.05; the results show 1.8(4) H *apfu*.

After the model was refined as above, difference-Fourier maps were examined around the 6*g* and 4*d* sites for any sign of electron density. None was seen, even when the experiment was repeated (with a different GS2 crystal) at a collection temperature of 100 K.

Crystal-structure refinement from neutron data

The fractional occupancy of Be at the *Be* site refined to 0.997(7). When Fe was placed at the *Be* site and the two atoms were properly constrained and refined to determine fractional occupancy, the occupancy of Be refined to above 1.0 and the fractional occupancy of Fe refined to below 0.0. It does not appear that Fe is replacing any of the Be at the *Be* site.

The electron-microprobe data indicate a significant amount of Mg in the sample, most likely occupying the *Al* site. Since the Fe content at this site is of the most

interest for this sample, results of the EMPA analyses were used to help in this determination. An average proportion of Mg:Al:Fe equal to 0.129:0.678:0.192 was determined from the sample used for diffraction. The Fe fractional occupancy was then set to 0.192. As fractional occupancies of three atoms at one site cannot be refined independently, we decided to create a "new" Al atom (Al* = Mg + Al) that would account for a constant Mg:Al ratio of 0.160:0.840. A new scattering length $b(\text{Al}^*) = 0.160 \cdot b(\text{Mg}) + 0.840 \cdot b(\text{Al}) = 0.160 \cdot 0.5375 + 0.840 \cdot 0.3449 = 0.3757$ was calculated for the new Al*, and the scattering length of Al in GSAS and SHELX was edited to reflect this change. The sum of Al* and Fe were constrained to sum to full-site occupancy, and fractional occupancies were refined to give results of 1.66(3) for Al* and 0.34(3) for Fe. These are similar to the values obtained from refinement of the single-crystal X-ray data (see above), and once again show ~0.1 *apfu* less Fe than the electron-microprobe-derived compositions.

The fractional occupancy of Si at the *Si* site refined to 0.998(7). Placing Be or Fe at this site and properly constraining the atoms gave the same result seen above for the *Be* site. It does not appear that either Be or Fe is replacing Si at the *Si* site. For Be (above) and Si, the fractional occupancies were set to full occupancy and were not refined further.

The fractional occupancy of the Na atom refined to 0.44(3). No Fe could be refined at the *Na* position.

The fractional occupancy of water in the channel refined to 0.91(2). No Fe could be modeled at the OW position. Negative scattering density indicating H

TABLE 5. INTERATOMIC DISTANCES (Å) AND ANGLES (°) FOR DARK BLUE BERYL

	X-ray	Neutron		X-ray	Neutron
Be – O(2) × 4	1.6514(7)	1.6465(7)	O(2) – Be – O(2)c × 2	92.96(5)	92.54(5)
<Be – O>	1.6514	1.6465	O(2) – Be – O(2)d × 2	108.48(5)	108.70(5)
Al – O(2)a × 6	1.9547(7)	1.9417(8)	O(2) – Be – O(2)e × 2	129.15(5)	129.42(4)
<Al – O>	1.9547	1.9417	<O – Be – O>	110.20	110.22
Si – O(1)	1.608(1)	1.603(1)	O(2)a – Al – O(2)f × 3	89.64(4)	89.72(4)
Si – O(1)b	1.606(1)	1.603(1)	O(2)a – Al – O(2)g × 3	75.56(4)	75.58(4)
Si – O(2) × 2	1.6156(7)	1.6100(9)	O(2)a – Al – O(2)h × 6	97.72(3)	97.68(3)
<Si – O>	1.611	1.607	<O – Al – O>	90.16	90.17
Na – OW × 2	2.2999	2.2890(8)	O(1) – Si – O(1)b	105.21(8)	105.22(8)
Na – O(1) × 6	2.554(1)	2.547(1)	O(1) – Si – O(2) × 2	110.66(4)	110.64(5)
<Na – O>	2.490	2.483	O(1)b – Si – O(2) × 2	109.35(4)	109.42(5)
OW – H	0.9(2)	0.99(2)	O(2) – Si – O(2)	111.42(6)	111.31(8)
			<O – Si – O>	109.44	109.44
			O(1) – Na – OW × 6	90.00	90.00
			O(1) – Na – O(1)j × 6	120.00	120.00
			O(1) – Na – O(1)b × 6	60.00	60.00
			<O – Na – O>	90.00	90.00
			H – OW – H		102(1)

Equivalent positions: a: $y, \bar{x} + y + 1, z$; b: $y, \bar{x} + y, \bar{z}$; c: $\bar{x} + y + 1, y, \bar{z} + \frac{1}{2}$; d: $x - y, \bar{y}, \bar{z} + \frac{1}{2}$; e: $\bar{x} + 1, \bar{y}, z$; f: $x - y, \bar{y} + 1, \bar{z} + \frac{1}{2}$; g: $y, x, \bar{z} + \frac{1}{2}$; h: $\bar{x} + 1, \bar{y} + 1, z$; i: x, y, \bar{z} ; j: $\bar{x} + y, \bar{x}, z$.

atoms was seen surrounding the OW site. An H atom was placed at the positions where it was observed in the difference-Fourier map. The H atom is located at a general position, which generates 12 partially occupied sites about each OW, which has $6/m$ site symmetry. This leads to six orientations of disordered water molecules about each OW atom. The atom was refined with fractional occupancies constrained to total twice the occupancy of OW. Subsequent refinement of the isotropic thermal parameter for hydrogen suggests that this model is accurate, and it can be seen in Figure 1 that the model closely resembles that for water in a type-II site, thus confirming the observations of Artioli *et al.* (1993) for alkali-containing beryl, but contradicting the results of Artioli *et al.* (1995) for the hydrous and sodic blue beryl from Ireland. Although additional negative scattering density can be found around the location of the water molecule, these peaks are too far from OW to be chemically reasonable for an O–H bond.

Difference-Fourier maps around the O1 and O2 sites were examined carefully to determine how much, if any, hydrogen was present in the form of OH⁻. Most of these negative scattering vectors appear at distances too close to the oxygen atoms. When hydrogen atoms were placed at these sites and allowed to refine, the refinement was unsuccessful, resulting in negative fractional occupancy for the hydrogen atom or refining to positions not consistent with an O–H bond. Thus, these data do not appear to show significant OH occupancy at the oxygen sites.

After the model was refined as above, difference-Fourier maps were examined around the 6g and 4d sites for any nuclear density. A small amount of negative density at the noise level of the difference map was noted. As Fe has a positive scattering-length and no Ti was found in the electron-microprobe analyses (Ti has a negative scattering-vector of -3.44), we concluded that these sites are empty. Final difference-Fourier calculations also contain various dips and bumps throughout the map. None of these peaks could be modeled with any chemical reasonability.

DISCUSSION

The electron-microprobe-derived compositions show that beryl samples from the True Blue showing contain high concentrations of Fe, possibly more (up to ~ 0.1 apfu Fe) than can be accommodated at the Al site. Charge-balance considerations and Mössbauer spectra indicate the presence of both Fe²⁺ and Fe³⁺. The optical absorption and Mössbauer spectra and the results of the X-ray and neutron single-crystal refinements suggest that there is very little Fe at the tetrahedral or channel sites.

The darkest blue samples contain the most Fe. Previous authors (Platonov *et al.* 1978, 1979a, 1979b, 1979c, Taran & Rossman 2001) have proposed that the

color of blue beryl is due to intervalence charge-transfer (IVCT) between Fe²⁺ and Fe³⁺ cations. The anisotropy of the optical absorption spectra suggest that if the mechanism responsible for the color in our samples is IVCT, the vector between the ions involved must be oriented approximately parallel to *c*. As shown in Table 6, there are only four vectors that fit this criterion and have realistic interatomic distances. However, the Al–Al and Na–Na distances are both 4.600 Å, which is too large to permit substantial IVCT. This leaves the 4d–Al and 6g–Be distances, both 2.300 Å which, as previously pointed out by Platonov *et al.* (1978, 1979a, 1979b, 1979c), are in the correct range to produce the observed optical effects.

The 4d position is surrounded by four O(2) atoms in square planar coordination at distances of 1.891 Å. In addition, there are two Si, two Be, and two 6g positions at distances of 1.826, 2.300, and 2.682 Å, respectively; the Be positions are arranged above and below each 4d site, such that the 4d–Be vectors are parallel to *c*, whereas the 4d–Si and 4d–6g vectors are perpendicular to *c*. Given the close proximity of the Si positions (closer than any anion sites), which the diffraction experiments suggest are completely occupied by Si⁴⁺, it is difficult to conceive of substitution taking place at this site. The diffraction experiments also suggest that the Be sites are fully occupied by Be. For these reasons, we do not believe that IVCT takes place between the 4d and Be positions.

The 6g site is surrounded by six O(2) atoms in trigonal prismatic coordination at distances of 2.161 Å; the polyhedron volume is 10.02 Å³. In addition, there are two Al, three Si, and three 4d sites at distances of 2.300, 2.386, and 2.682 Å, respectively; the Al positions are arranged above and below each 6g site such that the 6g–Al vectors are parallel to *c*, whereas the 6g–Si and 6g–4d vectors are perpendicular to *c*. The 6gO₆ polyhedron shares {001} triangular faces with two AlO₆ octahedra, and is slightly larger than the AlO₆ octahedra, which have Al–O distances of 1.955 Å and octahedral volumes of 9.58 Å³. Those ions that substitute at the Al site thus could also substitute at the 6g position, but only in very small amounts, because of the need to maintain local charge-balance.

If the “excess” Fe is at the 6g position, why do we not see it either in the Mössbauer spectra or in difference-Fourier maps of the X-ray- and neutron-diffraction data? For the former technique, it is likely that any doublet arising from Fe in the 6gO₆ polyhedron is too similar to the Fe in the AlO₆ octahedra to be resolved for either Fe²⁺ or Fe³⁺. The diffraction techniques should be able to resolve 0.1 Fe apfu (which for *P6/mcc* and the 6g site corresponds to 0.43 *e*⁻), but this is a maximum, and the actual amount of “excess” Fe at the 6g site is probably much lower.

In principle, it should be possible to calculate the concentration of Fe involved in the IVCT process from

the intensity of the band using the Beer–Lambert law. The IVCT band has an absorbance of about 2.0 in the 700 nm region for a 0.683 mm thick slab of sample GS2 (Fig. 4). The molar absorption coefficient (ϵ) for the IVCT interaction in beryl, needed for this calculation, is not known. If we use a typical molar absorption coefficient established by Amthauer & Rossman (1984) for intervalence charge-transfer systems in silicate minerals with concentrated IVCT interactions ($\epsilon = 150$) and the average density (2.78) of the beryl from Rohtert *et al.* (2003), we calculate that there are 0.20 moles per liter of Fe pairs, corresponding to 0.8 wt.% Fe involved in the IVCT interaction. This corresponds to 0.08 *apfu* Fe in the intervalence interaction, of which half (0.04 *apfu*, 0.17 e^-) would potentially be at the interstitial site. Unfortunately, this amount of electron and nuclear density is probably too small to be seen on the difference-Fourier maps, and consequently we are unable to confirm that IVCT involving Fe at the 6g position is responsible for the blue color of our samples. Thus the definitive explanation of the blue color of beryl is still lacking.

ACKNOWLEDGEMENTS

We thank E.C. Sklute for her assistance with Mössbauer data processing, and P.C. Piilonen for useful discussions. The authors thank M. Parker for editing the manuscript. The manuscript was improved by comments from P.F. Zanazzi, K. Schmetzer, C. Aurisicchio, and R.F. Martin. Financial support was provided by the Natural Sciences and Engineering Research Council of Canada in the form of Research Grants to LAG, the National Science Foundation (USA) grants EAR-0337816 to GRR and EAR-0439161 to MDD, and by a White Rose Foundation grant to GRR.

REFERENCES

- ADAMO, I., GATTA, G.D., ROTIROTI, N., DIELLA, V. & PAVESE, A. (2008): Gemmological investigation of a synthetic blue beryl: a multi-methodological study. *Mineral Mag.* **72**, 799-808.
- AMTHAUER, G. & ROSSMAN, G.R. (1984): Mixed valence of iron in minerals with cation clusters. *Phys. Chem. Minerals* **11**, 37-51.
- ARTIOLI, G., RINALDI, R., STÄHL, K. & ZANAZZI, P.F. (1993): Structure refinements of beryl by single-crystal neutron and X-ray diffraction. *Am. Mineral.* **78**, 762-768.
- ARTIOLI, G., RINALDI, R., WILSON, C.C. & ZANAZZI, P.F. (1995): Single-crystal pulsed neutron diffraction of a highly hydrous beryl. *Acta Crystallogr.* **B51**, 733-737.
- AURISICCHIO, C., FIORAVANTI, G., GRUBESSI, O. & ZANAZZI, P.F. (1988): Reappraisal of the crystal chemistry of beryl. *Am. Mineral.* **73**, 826-837.
- BRAGA, G.C.B., GARG, V.K., DE OLIVEIRA, A.C., FREITAS, J.A., JR., KUZMAN, E. & GARG, R. (2002): Optical and Mössbauer study of Brazilian emeralds. *Phys. Stat. Sol. A* **194**, 36-46.
- CHAROY, B., DE DONATO, P., BARRES, O. & PINTO-COELHO, C. (1996): Channel occupancy in an alkali-poor beryl from Serra Branca, (Goiás, Brazil): spectroscopic characterization. *Am. Mineral.* **81**, 395-403.
- DA COSTA, G.M., DE OLIVEIRA POLLI, G., KAHWAGE, M.A., DE GRAVE, E., SABIONI, A.C.S. & MENDES, J.C. (2006): The effect of thermal treatment on the ^{57}Fe Mössbauer spectrum of beryl. *Phys. Chem. Minerals* **33**, 161-166.
- DELLA VENTURA, G., ROSSI, P., PARODI, G.C., MOTTANA, A., RAUDSEPP, M. & PRENCIPE, M. (2000): Stoppaniite, $(\text{Fe,Al,Mg})_4(\text{Be}_6\text{Si}_{12}\text{O}_{36})^*(\text{H}_2\text{O})_2(\text{Na},\square)$ a new mineral of the beryl group from Latium (Italy). *Eur. J. Mineral.* **12**, 121-127.
- DUCHI, G., FRANZINI, M., GIAMELLO, M., ORLANDI, P. & RICCOBONO, F. (1993): The iron-rich beryls of Alpi Apuane. Mineralogy, chemistry and fluid inclusion. *Neues Jahrb. Mineral., Monatsh.*, 193-207.
- FIGUEIREDO, M.O., PEREIRA DA SILVA, T., VEIGA, J.P., LEAL GOMES, C. & DE ANDRADE, V. (2008): The blue colouring of beryls from Licungo, Mozambique: an X-ray absorption spectroscopy study at the iron K-edge. *Mineral. Mag.* **72**, 175-178.
- FONTAN, F. & FRANSOLET, A.M. (1964): The blue magnesium-, iron-, and sodium-containing beryl of the Lassur mine, Ariège, France. *Bull. Minéral.* **105**, 615-620.
- GOLDMAN, S.D., ROSSMAN, G.R. & PARKIN, K.M. (1978): Channel constituents in beryl. *Phys. Chem. Minerals* **3**, 225-235.
- GONCHAROV, G.N., SAKHAROV, A.N. & SHAROV, A.S. (1985): Specific features of iron positioning structures of differently colored beryls from the data of Mössbauer and EPR spectroscopies. *Int. Conf. on the Applications of the Mössbauer Effect (Alma-Ata, Kazakhstan)* **5**, 1705-1711.
- HOLLAND, T.J.B. & REDFERN, S.A.T. (1997): Unit cell refinement from powder diffraction data: the use of regression diagnostics. *Mineral. Mag.* **61**, 65-77.
- HOWARD, J.A.K., JOHNSON, O., SCHULTZ, A.J. & STRINGER, A.M. (1987): Determination of the neutron absorption cross section for hydrogen as a function of wavelength with a pulsed neutron source. *J. Appl. Crystallogr.* **20**, 120-122.
- JACOBSON, R.A. (1976): A single-crystal automatic indexing procedure. *J. Appl. Crystallogr.* **9**, 115-118.
- KHAIBULLIN, R.I., LOPATIN, O.N., VAGIZOV, F.G., BAZAROV, V.V., BAKHTIN, A.I., KHAIBULLIN, I.B. & AKTAS, B. (2003): Coloration of natural beryl by iron ion implantation. *Nucl. Instr. Meth. Phys. Res. B* **206**, 277-281.

- LAGOIRO, L., GRAÇA, L.M., MAGELA, G., PERSIANO, A.I.C., PINHEIRO, M.V.B. & KRAMBROCK, K. (2004): Crystal chemistry of aquamarines: a case study in pegmatites hosted in migmatites from the NE of Minas Gerais State, Brazil. *In Applied Mineralogy* (M. Pecchio *et al.*, eds.), ICAM-BR, São Paulo, Brazil (517-519).
- LARSON, A.C. & VON DREELE, R.B. (2000): General Structure Analysis System – GSAS. *Los Alamos Nat. Lab., Rep.* **86-748**.
- LOEFFLER, B.M. & BURNS, R.G. (1978): Shedding light on the color of gems and minerals. *Am. Sci.* **64**, 636-647.
- LONG, G.J., CRANSHAW, T.E. & LONGWORTH, G. (1983): The ideal Mössbauer effect absorber thickness. *Mössbauer Effect Ref. Data J.* **6**, 42-49.
- NOWACKI, W. & PHAN, K.D. (1964): Composition quantitative de la bazzite de Val Strem (Suisse) déterminée par la microsonde électronique de Castaing. *Bull. Soc. fr. Minéral. Cristallogr.* **87**, 453.
- OTTOLINI, L., BOITAZZI, P. & VANNUCCI, R. (1993): Quantification of lithium, beryllium, and boron in silicates by secondary ion mass spectrometry using conventional energy filtering. *Anal. Chem.* **65**, 1960-1968.
- OTTOLINI, L., CÂMARA, F., HAWTHORNE, F.C. & STIRLING, J. (2002): SIMS matrix effects in the analysis of light elements in silicate minerals: comparison with SREF and EMPA data. *Am. Mineral.* **87**, 1477-1485.
- PANKRATH, R. & LANGER, K. (2002): Molecular water in beryl, ${}^{\text{VI}}\text{Al}_2[\text{Be}_3\text{Si}_6\text{O}_{18}] \cdot n\text{H}_2\text{O}$, as a function of pressure and temperature: an experimental study. *Am. Mineral.* **87**, 238-244.
- PARKIN, K.M., LOEFFLER, B.M. & BURNS, R.G. (1977): Mössbauer spectra of kyanite, aquamarine, and cordierite showing intervalence charge transfer. *Phys. Chem. Minerals* **1**, 301-311.
- PEZZOTTA, F. (2001): *Madagascar: a Mineral and Gemstone Paradise*. ExtraLapis English No. 1, Lapis International, LLC, East Hampton, Connecticut, U.S.A.
- PLATONOV, A.N., POLSHIN, E.V. & TARAN, M.N. (1979a): On types of iron in beryls. *Zap. Vses. Mineral. Obshchest.* **108**, 725-730 (in Russian).
- PLATONOV, A.N., SHURIGA, T.N., GINSBURG, A.I., POLSHIN, E.V. & TARAN, M.N. (1979b): On an example of evolution of coloration of beryls in a process of formation of the deposit. *Constitution & Properties Minerals* **13**, 32-41 (in Russian).
- PLATONOV, A.N., TARAN, M.N., MINKO, O.E. & POLSHYN, E.V. (1978): Optical absorption spectra and nature of color of iron-containing beryls (A). *Phys. Chem. Minerals* **3**, 87-88.
- PLATONOV, A.N., TARAN, M.N., POLSHIN, E.V. & MINKO, O.E. (1979c): On nature of color of iron-bearing beryls. *Izvestiya Akad. Nauk SSSR, Seriya Geol.* **10**, 54-68 (in Russian).
- POUCHOU, J.L. & PITCHOIR, F. (1985): "PAP" $\phi(\rho Z)$ procedure for improved quantitative microanalysis. *In Microbeam Analysis* (J.T. Armstrong, ed.). San Francisco Press, San Francisco, California (104-106).
- PRICE, D.C., VANCE, E.R., SMITH, G., EDGAR, A. & DICKSON, B.L. (1976): Mössbauer effect studies of beryl. *J. Physique* **37**, C6-811-C6-817.
- PROCTOR, K. (1984): Gem pegmatites of Minas Gerais, Brazil: exploration, occurrence, and aquamarine deposits. *Gems & Gemology* **20**, 78-100.
- ROHTERT, W.R., QUINN, E.P., GROAT, L.A. & ROSSMAN, G.R. (2003): Blue beryl discovery in Canada. *Gems & Gemology* **39**, 327-329.
- SANDERS, I.S. & DOFF, D.H. (1991): A blue sodic beryl from southeast Ireland. *Mineral. Mag.* **55**, 167-172.
- SCHALLER, W.T., STEVENS, R.E. & JAHNS, R.H. (1962): An unusual beryl from Arizona. *Am. Mineral.* **47**, 672-699.
- SCHMETZER, K. & BERNHARDT, H.-J. (1994): Isomorphic replacement of Al and Si in tetrahedral Be and Si sites of beryl from Torrington, NSW, Australia. *Neues Jahrb. Mineral., Monatsh.*, 121-129.
- SCHULTZ, A.J. (1987): Pulsed neutron single-crystal diffraction. *Trans. Am. Crystallogr. Assoc.* **23**, 61-69.
- SCHULTZ, A.J., SRINIVASAN, K., TELLER, R.G., WILLIAMS, J.M. & LUKEHART, C.M. (1984): Single-crystal time-of-flight neutron-diffraction structure of hydrogen *cis*-Diacetylteracarboxylrheneate, $[\text{cis}-(\text{OC})_4\text{Re}(\text{CH}_3\text{CO})_2]\text{H}$: a metalla-acetylacetone molecule. *J. Am. Chem. Soc.* **106**, 999-1003.
- SCHULTZ, A.J., VAN DERVEER, D.G., PARKER, D.W. & BALDWIN, J.E. (1990): Structure of methylenecyclopropane-2-carboxamide by time-of-flight neutron diffraction. *Acta Crystallogr.* **C46**, 276-279.
- SEARS, V.F. (1986): Neutron scattering in condensed matter research. *In Methods of Experimental Physics* **23** (K. Sköld & D.L. Price, eds.). Academic Press, New York, N.Y. (521-550).
- SHELDRIK, G.M. (1997): *SHELXL-97 – a Program for Crystal Structure Refinement* (release 97-2). University of Göttingen, Göttingen, Germany.
- SHERRIFF, B.L., GRUNDY, H.D., HARTMAN, J.S., HAWTHORNE, F.C. & ČERNÝ, P. (1991): The incorporation of alkalis in beryl: multi-nuclear MAS NMR and crystal-structure study. *Can. Mineral.* **29**, 271-285.
- TARAN, M.N., KLYAKHIN, V.A., PLATONOV, A.N., POL'SHIN, É.V. & INDUTNYI, V.V. (1989): Optical spectra of natural and artificial iron-containing beryls at 77–297 K. *Sov. Phys. Crystallogr.* **34**, 882-884.
- TARAN, M.N. & ROSSMAN, G.R. (2001): Optical spectroscopic study of tuhualite and a re-examination of the beryl, cordierite, and osumilite spectra. *Am. Mineral.* **86**, 973-980.

- TURNER, D. (2006): *Mineralogical and Geochemical Study of the True Blue Aquamarine Showing, Southern Yukon*. M.Sc. thesis, Univ. British Columbia, Vancouver, British Columbia.
- TURNER, D., GROAT, L.A., HART, C.J.R., MORTENSEN, J.K., LINNEN, R.L., GIULIANI, G. & WENGZYNOWSKI, W. (2007): Mineralogical and geochemical study of the True Blue aquamarine showing, southern Yukon. *Can. Mineral.* **45**, 202-227.
- VIANA, R.R., DA COSTA, G.M., DE GRAVE, E., JORDT-EVANGELISTA, H. & STERN, W.B. (2002a): Characterization of beryl (aquamarine variety) by Mössbauer spectroscopy. *Phys. Chem. Minerals* **29**, 78-86.
- VIANA, R.R., JORDT-EVANGELISTA, H., DA COSTA, G.M. & STERN, W.B. (2002b): Characterization of beryl (aquamarine variety) from pegmatites of Minas Gerais, Brazil. *Phys. Chem. Minerals* **29**, 668-679.
- YOUNG, R.A., SAKTHIVEL, A., MOSS, T.S. & PAIVA-SANTOS, C.O. (1995): DBWS9411 – an upgrade of the DBWS* programs for Rietveld refinement with PC and mainframe computers. *J. Appl. Crystallogr.* **28**, 366-367.
- WOOD, D.L. & NASSAU, K. (1968): The characterization of beryl and emerald by visible and infrared absorption spectroscopy. *Am. Mineral.* **53**, 777-800.

Received September 7, 2007, revised manuscript accepted June 6, 2010.

APPENDIX

A fully automated CAMECA SX-50 electron microprobe was used for analysis (wavelength-dispersion mode). Operating conditions were as follows: excitation voltage 15 kV, beam current 20 nA, peak count-time 20 s, background count-time 10 s (Na, Al, Si), peak count-time 50 s, background count-time 25 s (other elements), spot diameter (standards and specimen), 30 μm . Data reduction was done using the "PAP" $\phi(\rho Z)$ method (Pouchou & Pichoir 1985). Compositions were recalculated on the basis of 3 Be and 18 O *apfu*.

Secondary ion mass spectrometry (SIMS) analyses were done with a Cameca IMS 4f ion microprobe. Instrumental conditions were similar to those in Ottolini *et al.* (2002). Five analytical cycles were used and $^1\text{H}^+$, $^7\text{Li}^+$, $^9\text{Be}^+$, $^{11}\text{B}^+$, $^{27}\text{Al}^+$, and $^{30}\text{Si}^+$ were detected together in each cycle. A homogeneous crystal of danalite was used to calibrate the Be $^+$ /Si $^+$ ion signal ratios, which showed an overall instrumental uncertainty (mostly related to the stability of the primary-beam current intensity) of <0.1% relative over the five analytical cycles. We used working curves for silicates from Ottolini *et al.* (1993) for the Li and B calibration. $^{30}\text{Si}^+$ was used as the internal standard for Li, Be, and B, and $^{27}\text{Al}^+$ was used as the internal reference for H. Concentrations of trace elements (Sc, Ti, V, Cr, Sr, Zr, Nb, Ba, REE, and Hf) were measured at four spots on two crystals from sample 46.

Laser-Ablation Microprobe (LAM)-ICP-MS compositions were obtained with a Thermo XSI-X7 ICP-MS with a Merchantek Minilase II laser-ablation microprobe. When fired, the laser delivered light energy (normally 1 to 2.5 mJ) in pulses (1 to 20 Hz) at a wavelength of 266 nm. A spot size of approximately 50 μm was used. Background signals for each mass were measured on the carrier gas blank prior to, and after, firing the laser. Drift, matrix effect, changes in

laser sampling yield, and transport efficiency during the analysis were corrected for by using Al as an internal standard. Elemental concentrations were determined by analyzing glasses from the National Institute of Standards and Testing.

Polarized optical absorption spectra were obtained with the diode array microspectrophotometer described by Taran & Rossman (2001). Analysis spots were typically 100 \times 100 μm taken through the clearest portions of a room-temperature sample, which was doubly polished on [100]. Near-IR spectra and mid-IR spectra were obtained using a Nicolet 860 FTIR with LiIO₃ crystal polarizers, CaF₂ beam splitter and a LN₂-cooled MCT-A detector. Analysis spots were 600 μm diameter in area in the clearest portion of the sample. Spectra were obtained from the beryl sample studied plus a series of previously oriented samples of beryl available at the California Institute of Technology.

For the Mössbauer study, optically pure crystals of beryl were weighed and then crushed to fine powders under acetone to avoid heating and potential oxidation. The samples were then mixed with sucrose, also under acetone, before placement into a sample holder confined by Kapton tape. The resultant thickness of the sample was 1.37 mg Fe/cm², roughly at the thin-absorber thickness approximation of Long *et al.* (1983), but high enough for acquisition of a useful spectrum.

Mössbauer spectra were acquired at 4, 12, 80, and 295 K using a source of ~90 mCi ^{57}Co in Rh on a WEB Research Co. model WT302 spectrometer equipped with a Janus He cryostat. Run times were 1-2 days. Results were calibrated against an α -Fe foil of 6 μm thickness and 99% purity. For each sample, the fraction of the baseline due to the Compton scattering, 122 keV gammas, by electrons inside the detector was subtracted. Experiment times were 12-24 hours, and

baseline counts were ~ 2 million after the Compton correction, as needed to obtain reasonable counting statistics. Spectra were collected in 1048 channels and corrected for nonlinearity *via* interpolation to a linear scale of velocity defined by the spectrum of the 25 μm Fe foil used for calibration. Data were then folded before fitting.

The spectra were fit using the MEX_FIELDDD program, which uses Lorentzian line shapes and solves full Hamiltonians for isomer shift and quadrupole splitting distributions in each of two valence states. Isomer shift (δ), and quadrupole splittings (Δ) of the doublets were allowed to vary, and widths of all four peaks were coupled to vary in unison. Errors on isomer shift and quadrupole splitting of well-resolved peaks are usually ± 0.02 mm/s, and these are probably realistic for the dominant Fe^{2+} doublet. For the sextets and the smaller Fe^{3+} doublets, errors based on repeated fits to the data are ± 0.05 mm/s for δ and ± 0.1 mm/s for Δ owing to heavy overlap of peaks. Errors on peak areas based on repeated fits using different constraints and fitting models are ± 1 –3% absolute. Thus, the detection limit for Fe^{3+} in this sample is estimated at ± 1 –3%.

Powder X-ray-diffraction experiments were done with a Siemens D5000 diffractometer equipped with a diffracted-beam graphite monochromator, incident beam Soller slit, 2 mm divergence and antiscatter slits, and a 0.6 mm receiving slit. The normal-focus Cu X-ray tube was operated at 40 kV and 30 mA. Powder-diffraction data were collected over ranges of 10 to 70° 2 θ , using scanning steps of 0.02° 2 θ . Peak positions plus the internal standard mixture were measured by Rietveld refinement using the program DBWS-9807 (Young *et al.* 1995). The $\text{CuK}\alpha_1$ peaks were corrected for cell refinement by reference to the internal standard. Unit-cell dimensions were determined from the corrected X-ray powder-diffraction data using the program UNITCELL (Holland & Redfern 1997).

Single-crystal X-ray-diffraction measurements were made using a Bruker X8 APEX diffractometer with graphite-monochromated $\text{MoK}\alpha$ radiation. The data were collected at room temperature to a maximum 2 θ value of 60.2°. Data were collected in a series of ϕ and ω scans in 0.50° oscillations with 10.0 second exposures. The crystal-to-detector distance was 40 mm. Data were collected and integrated using the Bruker SAINT software package. Data were corrected for absorption effects using the multi-scan technique (SADABS). The data were corrected for Lorentz and polarization effects. All refinements were performed using the SHELXTL crystallographic software package of Bruker AXS. The structure was refined using starting parameters from Artioli *et al.* (1993). All non-hydrogen atoms were refined anisotropically.

Neutron-diffraction data were obtained at the Intense Pulsed Neutron Source (IPNS) at Argonne National

Laboratory using the time-of-flight Laue single-crystal diffractometer (SCD) (Schultz *et al.* 1984, Schultz 1987). Details of the data collection and analysis procedures are given in Schultz *et al.* (1990). A crystal from the GS2 sample was ground to an approximate sphere ($2 \times 2 \times 3$ mm³) then wrapped in aluminum foil and glued to an aluminum pin that was then mounted on the cold stage of a closed-cycle helium refrigerator and cooled to 40 ± 1 K. For each setting of the diffractometer angles, data were stored in three-dimensional histogram form with coordinates x,y,t corresponding to horizontal and vertical positions of the detector and the time-of-flight, respectively. An auto-indexing algorithm (Jacobson 1976) was used to obtain an initial orientation matrix from the peaks in three preliminary histograms measured for 30 minutes each. For intensity-data collection, experiments of three hours per histogram were initiated for the dataset. Settings were arranged at χ and ϕ values suitable to cover at least one unique twelfth of reciprocal space (Laue symmetry $6/mmm$). With the counting times stated above, 13 histograms were completed for the three days available for the experiment. The recorded histograms were indexed and integrated using individual orientation matrices for each histogram, to allow for any misalignment of the sample. Intensities were integrated about their predicted locations and were corrected for the Lorentz factor, the incident spectrum, and the detector efficiency. A wavelength-dependent spherical absorption correction was applied using cross sections from Sears (1986) for the nonhydrogen atoms and from Howard *et al.* (1987) for the hydrogen atoms [μ (cm⁻¹) = $0.497 + 0.126 \lambda$]. Symmetry-related reflections were not averaged since different extinction-factors are applicable to reflections measured at different wavelengths.

The GSAS software package was used for the initial structural analysis (Larson & Von Dreele 2000). The atomic positions of the X-ray diffraction structure (see above) except for H atoms were used as a starting point in the refinement. Once the basic structure was refined and the refinement of the extinction parameter had converged, the extinction-corrected data were used to refine the final model with SHELX97 (Sheldrick 1997), where equivalent peaks were merged. The H atoms were located in a difference-Fourier map during these stages of refinement. The refinement was based on F^2 reflections with a minimum d -value of 0.5 Å. Weights were assigned as $w(F_o^2) = 1/[\sigma^2(F_o^2) + (F_o^2)]^2$, where $\sigma^2(F_o^2)$ is the variance based on counting statistics. In the final refinement, all non-hydrogen atoms were refined with anisotropic displacement parameters. After the final refinement, the minimum and maximum peaks of unmodeled scattering density in the difference-Fourier map were 0.320 and 0.290 fm Å⁻³, respectively, which compare to approximately 1.8% or less of the peak height of Be in a Fourier map.

